Supplementary Information for:

An Efficient Off-Membrane Switch: Par6 Facilitates Processive Phosphorylation of Lgl's Serine Sites via a Dynamic Interaction with aPKC

Lior Almagor[1,2]* and William I. Weis[1,2#]

Departments of [1]Structural Biology and [2]Molecular & Cellular Physiology, Stanford University School of Medicine, Stanford, CA 94306 USA

[#] Deceased
* Correspondence: lalmagor@stanford.edu

A

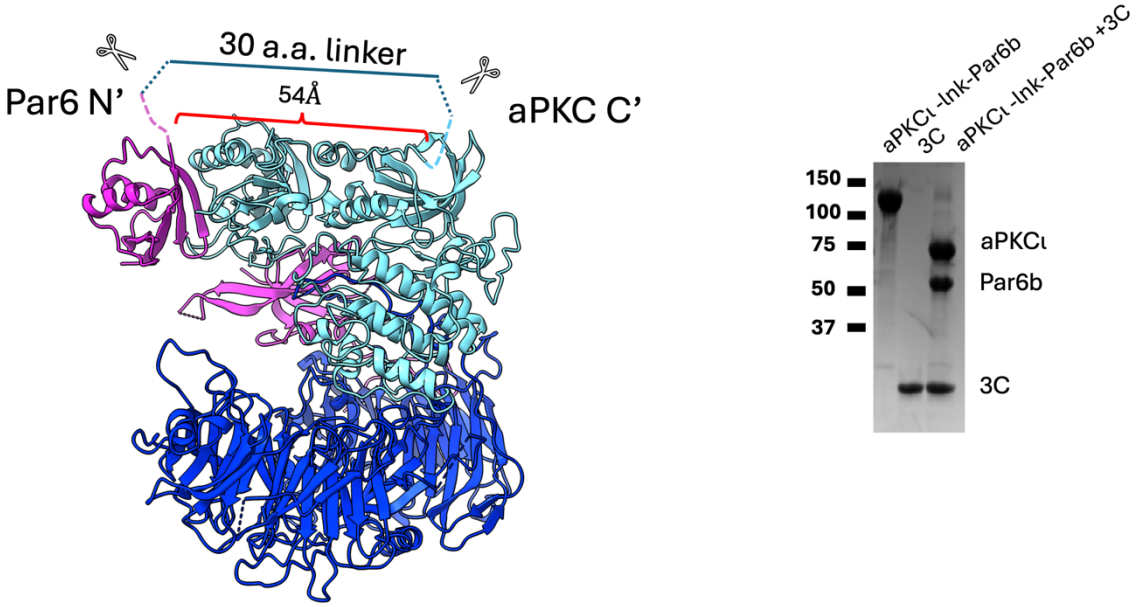

B

E:		S1: Lgl2(638-666)	S2: Lgl2s	S2: Lgl2s(I700D)
aPKCι-lnk-Par6b	[a]Kcat (min-1)	67.0 ± 3.0	7.7 ± 0.4	23.2 ± 0.5
	[a]Km (μM)	1.75 ± 0.35	0.13 ± 0.04	0.23 ± 0.02
	[Et] (nM)	154.5	154.5	154.5
	[s] (nM)	393900.0	40.0	40.0
	V (nM/min)	**10283.6**	**1.7**	**2.7**
aPKCι	[a]Kcat (min-1)	84.5 ± 5.8	32.0 ± 0.5	28.2 ± 0.4
	[a]Km (μM)	3.58 ± 0.94	0.74 ± 0.06	0.74 ± 0.04
	[Et] (nM)	154.5	154.5	154.5
	[s] (nM)	393900.0	40.0	40.0
	V (nM/min)	**12923.8**	**2.4**	**2.1**

Figure S1 (supplementary). aPKCι-Par6b fusion and in-vitro kinase assays. (related to Figure 2).

A. The structure-based designed aPKCι-lnk-Par6b fusion construct. A 30 amino acid long protein linker was inserted between aPKCι's C-terminus to Par6's N-terminus. The distance between these termini, which are presented on the top surface of the Lgls2/aPKCι/Par6 complex as shown in the nucleotide-free structure, is 54 Å. With the addition of 15 and 8 residues, which are naturally unstructured in the Par6b and aPKCι N- and C- termini, respectively, the peptide chain linking between these points in the structure includes 53 amino acids. A flexible linker at this length can cover this distance multiple times and allows the domain arrangement as observed in the structure. The linker contains 3C protease sites at both ends that could be used to isolate the fused proteins by proteolysis, as observed in the gel. **B.** Calculation of the expected rates of phosphorylation of the fluorescently labeled Lgl2s (S2) proteins and the excessively added Lgl2(638-666) decoy peptides (S1) based on their ratios and the kinetic parameters determined for each with either aPKCι or aPKCι-link-Par6b (E). The rates (V) are

calculated for distributive phosphorylation, where, in every cycle, the enzyme could pick either of the substrates (S1 or S2). For such a mechanism, the wildtype labeled Lgl2s phosphorylation should have similar rates (and even higher) with aPKC compared to the aPKCι-Par6b fusion. However, in the experiment, the reaction with Par6 achieves multisite phosphorylation faster. For the Lgl2s I700D mutant, similar reaction rates are also expected (even faster with Par6). However, in the experiment, the reaction with the Par6b fusion doesn't reach multisite phosphorylation as fast as with wildtype Lgl2s, which may result from an interfered mechanism of processivity.

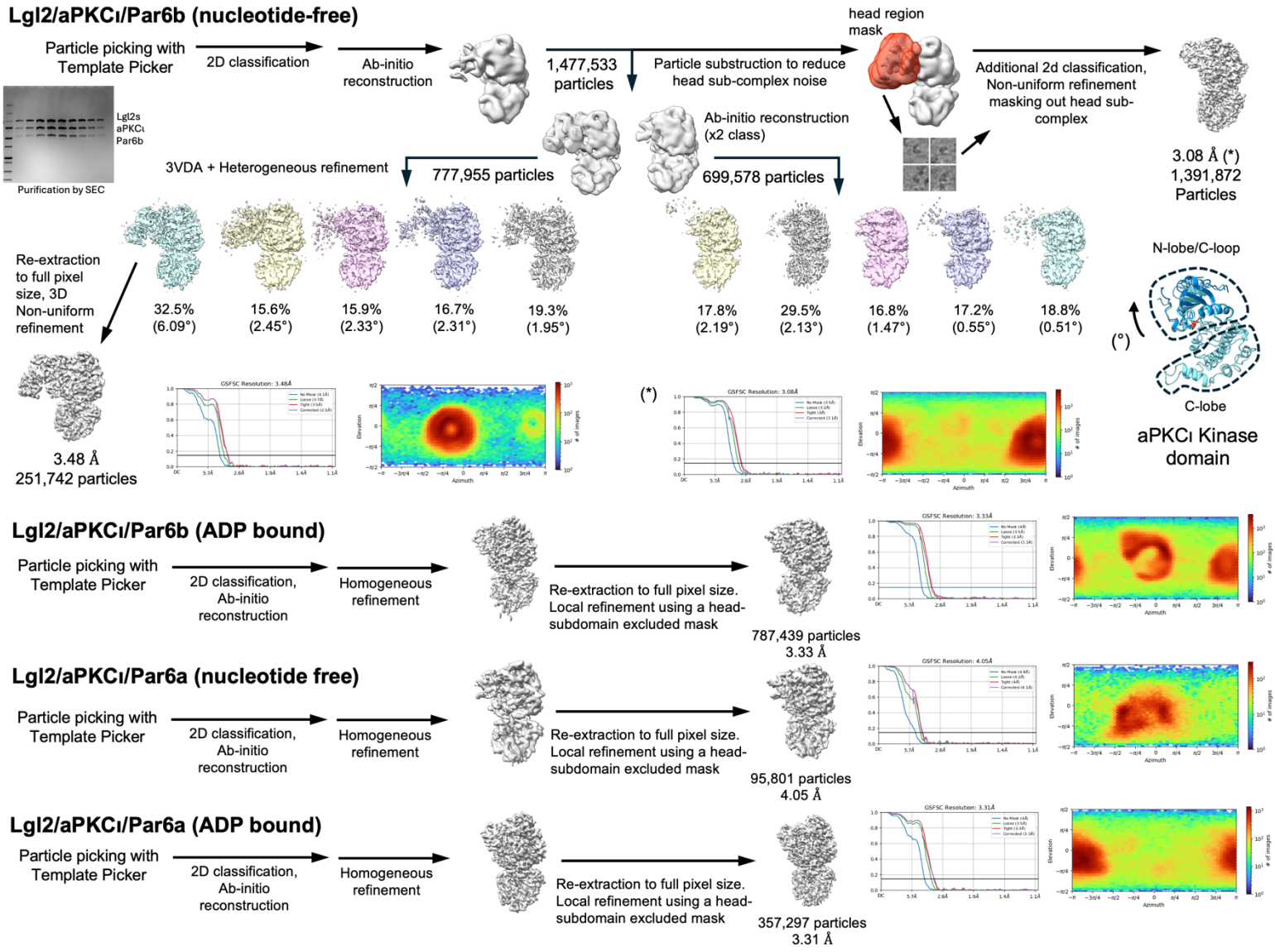

Figure S2 (supplementary). Particle subset selection and refinement of the Lgl2/aPKCι/Par6b and Lgl2/aPKCι/Par6a cryo-EM structures. (related to Figures 3 and 5).

A scheme representing the processing strategy used to generate each cryo-EM map. The volume region that includes the interacting PKCi's PB1-C1 and Par6's PB1 (the head sub-complex) showed high flexibility against the rest of the complex's regions in all of our data. For the nucleotide-free Lgl2s/aPKCι/Par6b data, isolation of a subset of particles that present an interpretable map region was possible using Cryosparc's 3D variability analysis (3DVA) followed by heterogeneous refinement with input volumes generated by 3VDA clustered results. The different classes generated presented some variation in the relative angles between the aPKCι N-lobe/C-loop region and its C-lobe. The selected class, showing the head sub-complex had the kinase lobes at their mostly open conformations. Denoted under each class are the N-lobe/C-loop angle changes measured relative to its position in the ADP bound Lgl2s/aPKCι/Par6b structure with a closed kinase conformation. The Par6b PDZ's position relative to Lgl2 also

varied between classes. The following angle changes measured relative to the leftmost class's PDZ (left to right): 4.32°, 4.85°, 6.85°, 1.26°, 7.18°, 4.13°, 7.04°, 7.49°, and 3.31°. The change in the relative angle between the aPKC domains was measured by separately fitting aPKCι's N-lobe/C-loop and its C-lobe models into refined maps generated from each class (Cryosparc Homogeneous Refinement). The generated models, aligned by their C-lobes, were then measured using Pymol's 'angle_between_domains' function. The PDZ angles were similarly measured. Note that these measurements using rigid body fitting are for illustration purposes only and are not intended to measure precise angles between domains.

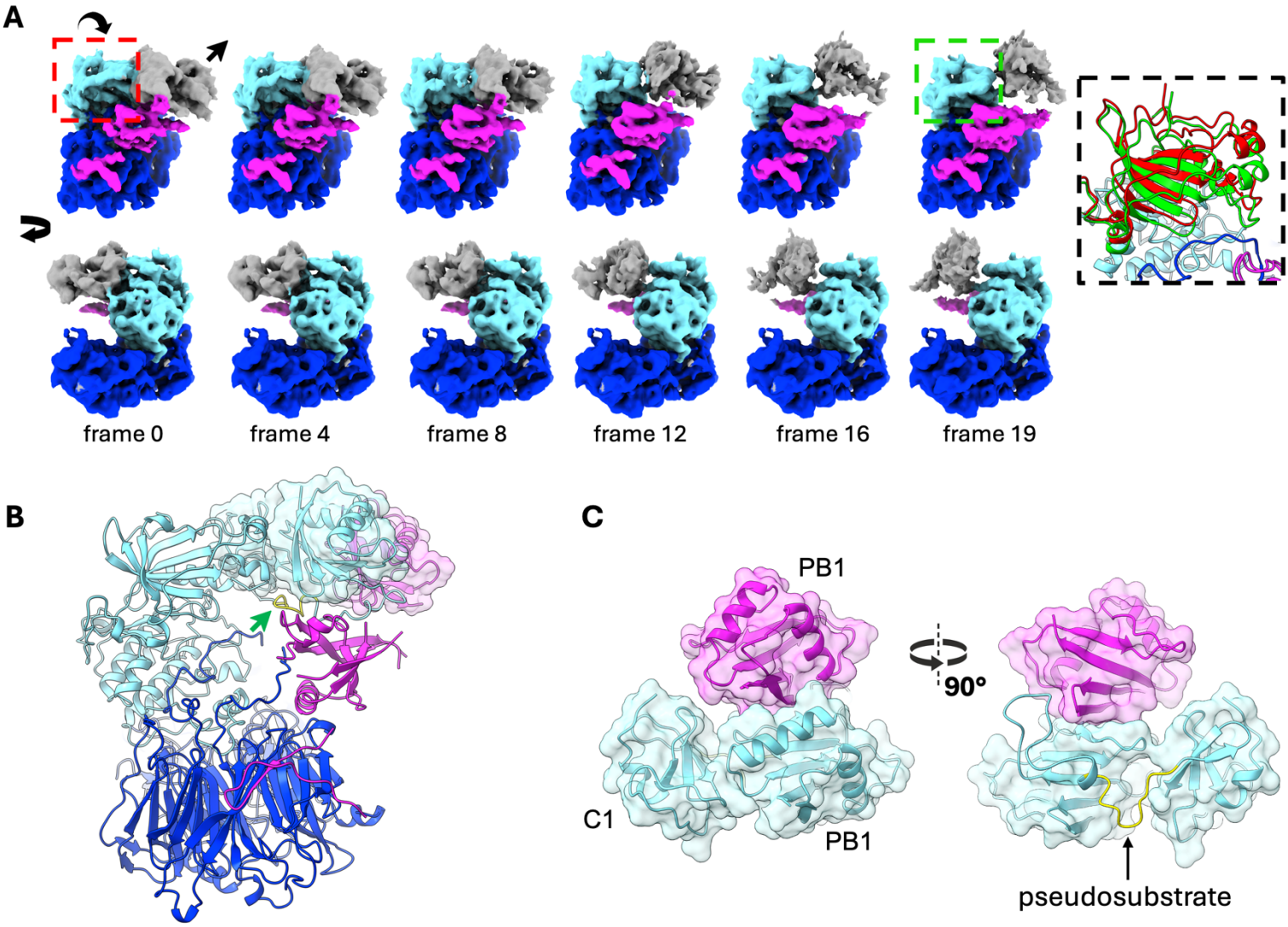

Figure S3 (supplementary). Conformational variability in the nucleotide-free Lgl2/aPKCι/Par6b structure and the head sub-complex (related to Figure 3).
A. 3D variability analysis of the empty Lgl2s/aPKCι/Par6b cryo-EM data. Selected frames from component-2 of the analysis. Two opposite viewpoints are shown. The volume regions are colored with Lgl2 in blue, aPKCι in cyan, and Par6b in magenta. A closing movement of the kinase N-lobe/C-loop observed in this series of frames is emphasized by comparing their positions between frames 0 (red) and 19 (green). The head dislocates from the complex with the closing of the kinase lobes. **B.** The Lgl2s/aPKCι/Par6b complex with the head sub-complex Lgl2 is in blue, aPKCι in cyan, and Par6b in magenta. The green arrow points to the aPKCι pseudo-substrate region (marked yellow). **C.** The aPKCι/Par6b head sub-complex. Presented in ribbon only is the aPKCι protein chain linking the PB1 and C1 domains, which include the pseudo-substrate region, that passes at the bottom side of the head sub-complex.

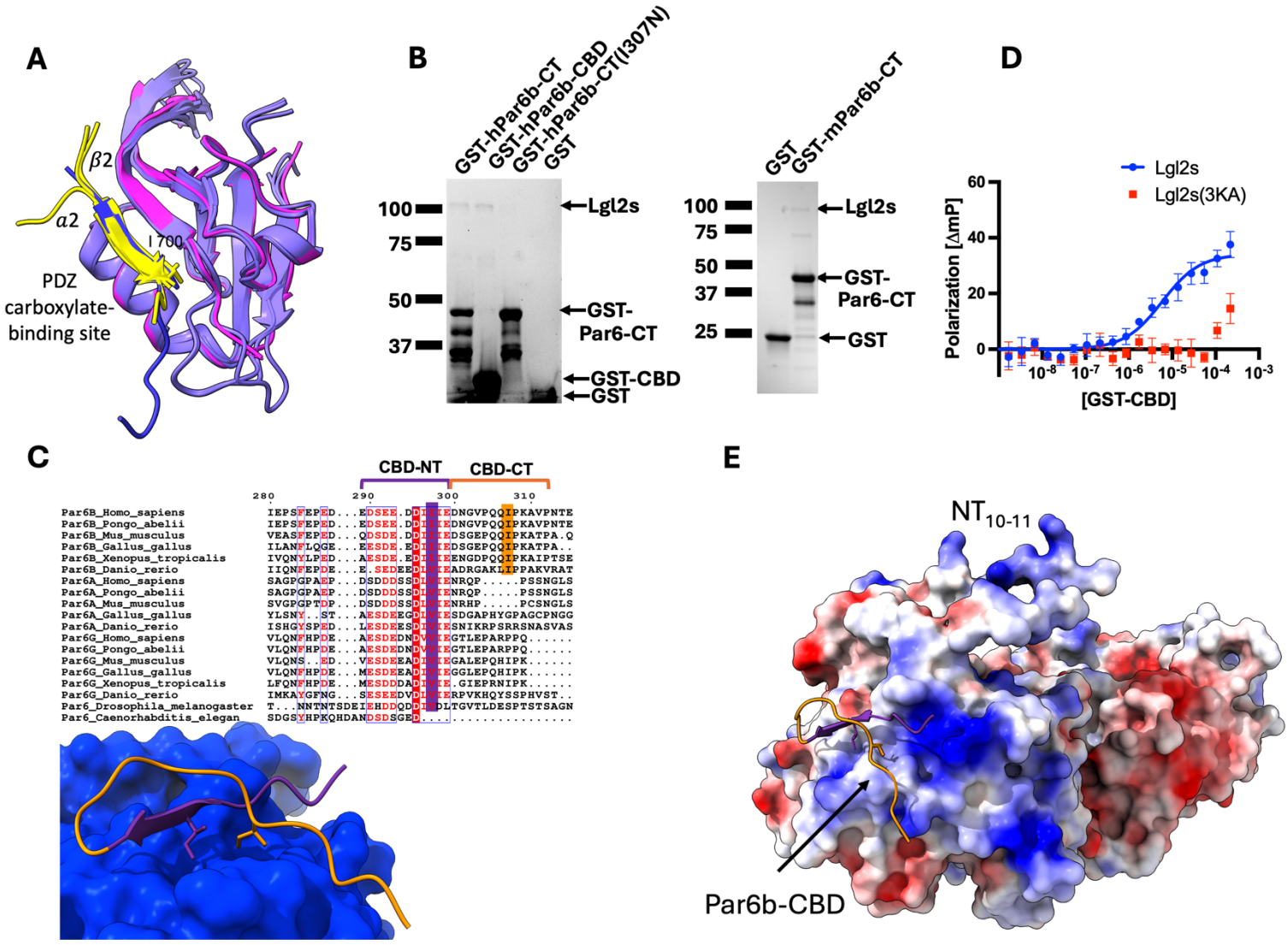

Figure S4 (supplementary). The Lgl2/Par6b interaction. (related to Figure 4).
A. Comparison of the Lgl2 10-11 loop's interaction with the Par6 PDZ to other PBM/PDZ interactions. Structural alignment of the Par6b/Lgl2 CT10-11 interface with previously published structures of Par6 PDZ in complex with different PBMs (PDB IDs: *1X8S, 5I7Z, 1RZX*). The Par6b/Lgl2 is in magenta/blue, while in the others, the PDZ is in purple, and PBM is yellow. The hydrophobic PBMs' C-terminal residues (internal in Lgl2's case (I700) as well as in Pals1) are shown in stick representation. **B.** Par6b's C-terminus directly interacts with Lgl2. Left: A pull-down assay with glutathione agarose beads, comparing the binding of GST and GST fused fragments of human Par6b C-terminal fragments to Lgl2s. Both the GST-hPar6b-CT complete tail (254-271) and the GST-hPar6b-CBD isolated CBD (289-312), but not GST specifically bind Lgl2s (lanes 1, 2, 4). The I307N mutation abolishes the Par6 C-terminus/Lgl2 interaction (compare lanes 3 and 1). Right: A similar Pulldown experiment using a homologous fragment (254-371) from mouse Par6b used in this study. **C.** Conservation of Par6's CBD. Multiple sequence alignment of representative Par6 sequences focused on the region around Par6b's

CBD. Marked are the N-terminal (CBD-NT) and C-terminal (CBD-CT) halves of the Par6b CBD. The halves are marked with the same colors as in the CBD structure figure on the right. The positions of I297 and I307, which are important for the CBD's Lgl2 binding, are marked in purple and orange, respectively. **D.** FP experiments. Wild-type Lgl2s specifically interact with GST-CBD, while this interaction is abolished by mutating Lgl2's K820A, K832A, and K834A (3KA). **E.** Lgl2 surface potential (red, negative; blue, positive). Lgl is shown in surface representation, colored by the potential scale. Par6b CBD is presented in ribbon, colored as in C. Note the positive patch close to Lgl's interface with Par6b's CBD-NT rich with negatively charged residues.

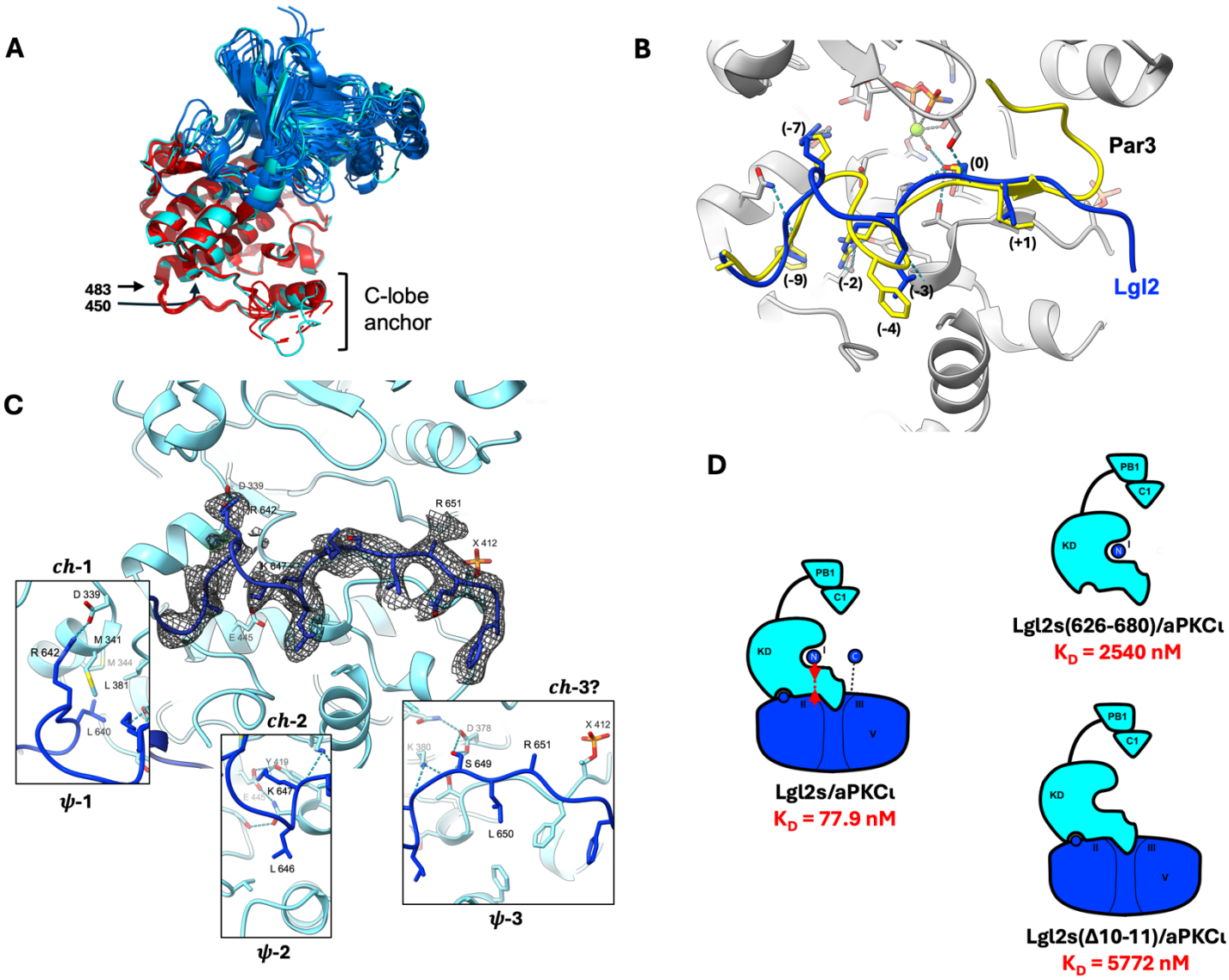

Figure S5 (supplementary). The Lgl2/aPKCι interaction. (related to Figure 5).
A. aPKCι C-lobe anchor (residues 450-483) comparison with other structures. Structural alignment of the aPKCι KD from the structure (cyan) with those of previously determined aPKCι KD crystal structures (PDB ids: *3A8W, 3ZH8, 4DC2, 5LI1, 3A8X, 5LI9*). The alignment was performed via the KD C-lobe. N-lobe/C-loop of reference structures is colored blue, and C-lobe is red. **B.** Comparison of aPKCι KD's Lgl2 and par3 substrate binding. A structure alignment of the aPKCι/Lgl2 NT10-11 interaction from the nucleotide-free Lgl2s/aPKCι/Par6b structure to the crystal structure of the AMP-PNP bound aPKCι KD with Par3(816-841)[2]. The aPKCι/Par3 structure is in gray/yellow, Lgl2 is in blue. The alignment was performed via the KD C-lobes in both structures, but the aPKCι from the complex with Lgl2 is omitted for clarity. Lgl2 residues 638-650 show structural homology to Par3(816-828), and some of the important elements of this interface are similar between them. This includes the hydrophobic and polar interactions of Lgl2 L640/Par3 F818 (position (-9)) and Lgl2 R642/Par3 R820 (position (-7)) with aPKCι's ψ-1 and Ch-1. Also, the important substrate positions (-2) to (+1), K647-L560 (positions -3, -2, 0, +1) of

Lgl2 and R825-M828 (positions -4, -2, 0, +1) of Par3, take part in similar interactions with the active site. Unlike the Par3 peptide, whose C-terminal part (829-841) folds back and interacts with the aPKC activation loop, αB and αC helices, the Lgl2 NT10-11 does not change its direction and runs parallel to aPKC P+1 until it exits the interface with the KD. **C.** The Lgl2 10-11 loop's interaction with aPKCι (interface (I)) in the nucleotide-free structure. Interaction of the NT10-11 with aPKCι KD active site's ψ-1-3 and charge-1-3 sites, based on the classification used by Wang et al [3] (our definition of the charge-3 site is different). Our model with S649 at position S0 fits the EM volume data. However, the local low quality of the data may be due to a possible mixed population of different Lgl2 serine sites populating the active site. Data are insufficient to determine the rotamer of Lgl2's R651 in the model that could possibly interact with the phosphate group on T412. **D.** The high affinity of Lgl2 to the nucleotide-empty aPKC requires cooperation between the top (I) and bottom (II) interaction sites. Cartoon figures representing FP experiments between FL aPKCι and Hylight488 labeled Lgl2 constructs.

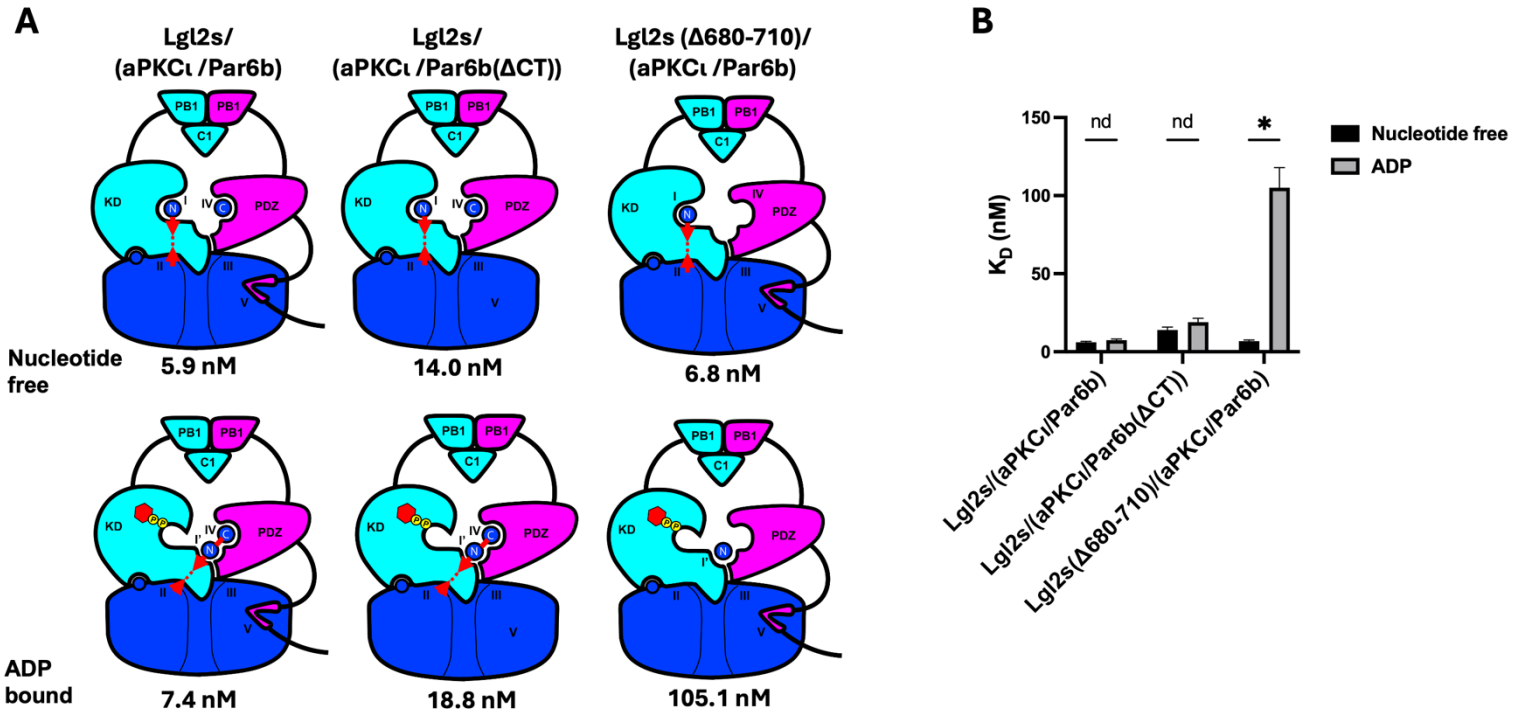

Figure S6 (supplementary). Cooperation with Par6b allows the continuous high-affinity binding of Lgl2 and aPKCι KD between the nucleotide-free and ADP-bound states. (related to Figure 5).

A-B. Cartoon figures **(A)** and chart **(B)** illustrating FP results of fluorescent Lgl2s binding to intact aPKCι/Par6b (left), to a truncated complex (aPKCι/Par6b(ΔCT)) missing Par6(254-371) (middle), and the binding of a fluorescent Lgl2s(Δ680-710), which has PBM removed, to aPKCι/Par6b (Right). The experiments were performed both in the nucleotide-free (top row) and the ADP-bound conditions (bottom row). The cooperation between aPKC's KD, Lgl2's $CT_{10\text{-}11}$, and Par6's PDZ that form the alternative site I' for Lgl2's $NT_{10\text{-}11}$ allows the high-affinity interaction in the ADP-bound state. This binding is still maintained even in the absence of the Lgl2/Par6-CBD interaction, while it is affected by the deletion of the Lgl2 CBD at its $CT_{10\text{-}11}$ (P= 0.001590). Unpaired t-test.

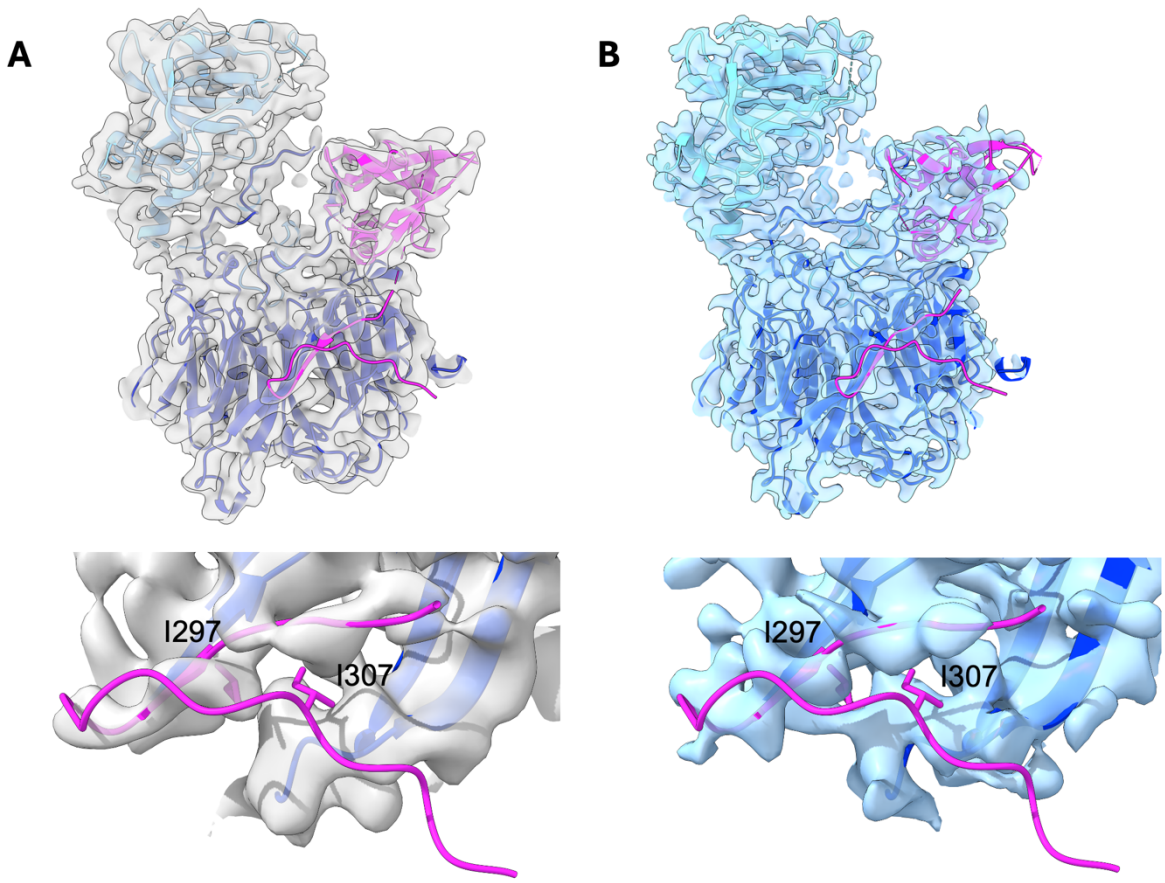

Figure S7 (supplementary). The Lgl2/aPKCι/Par6a cryo-EM data (related to Figure 6).
A-B. Top: Lgl2s/aPKCι/Par6a nucleotide-free **(A)** and ADP-bound **(B)** cryo-EM maps. The appropriate Lgl2s/aPKCι/Par6b models were aligned into the maps. **Bottom:** Close up on the map area near the aligned Par6b's CBD. The Lgl2s/aPKCι/Par6a maps show only some partial density around the CBD N-terminus half.

Probe immobilized	Binding partner	Nucleotide	Equallibrium K_D (nM)[a]	K_{on} ($M^{-1}s^{-1}$)	K_{off} (s^{-1})	K_{off} /K_{on} (nM)[b]	n[e]
Lgl2s	aPKCι	AMP-PNP	128.4 ± 18.2	14269 ± 644 [c]	0.0018 ± 0.0005 [c]	127.0	3
	aPKCι	ADP	95.9 ± 10.8	19756 ± 1045 [c]	0.0015 ± 0.0001 [c]	77.0	3
	aPKCι		74.8 ± 13.9	21645 ± 2598 [c]	0.0004 ± 0.0001 [c]	16.4	3
	aPKCι/Par6b	AMP-PNP	5.3 ± 0.6	111000 ± 5199	0.0008 ± 0.0001	7.6	3
	aPKCι/Par6b	ADP	5.0 ± 0.8	202900 ± 3719	0.0011 ± 0.0002	5.6	3
	aPKCι/Par6b		5.0 ± 0.5	230700 ± 4198	0.0014 ± 0.0001	6.1	3
	aPKCι-PB1/Par6a		16376 ± 3584	397 ± 57	0.0067 ± 0.0005	16914.2	1
pLgl2s	aPKCι	AMP-PNP	N.D.[d]				3
	aPKCι		N.D.[d]				3
	aPKCι/Par6b	AMP-PNP	76.5 ± 14.5	87450 ± 4409	0.0107 ± 0.0004	122.4	3
	aPKCι/Par6b		28.7 ± 3.5	147800 ± 8706	0.0058 ± 0.0003	39.0	4
Par6b	Lgl2s		41.03 ± 3.7	862800 ± 130300	0.0356 ± 0.0065	41.2	2
Par6a	Lgl2s		N.D.[d]				1

Binding affinities and rate constants determined by BLI. All values are given as mean ± SEM.

[a] Affinity determined from equilibrium binding signals.

[b] Affinity determined from the ratio of kinetic rate constants

[c] Kinetic rate constants were determined by fitting the association phase only

[d] Not detected. No quantifiable binding was observed in the range of binding partner concentrations tried.

[e] Number of replicated experiments, each done with between 6-9 binding partner concentrations around KD.

Table 1. Summary table of BLI binding experiments.

Labeled	Binder	KD (nM)	*n*	Lgl2 sites interferred/ ommited	Lgl2 binding sites available
Lgl2s	aPKCι	77.9 (66.2-91.5)	7		I-II
	aPKCι (Mg/ADP)	N.D.[a]	3		I-II
	aPKCι (Mg/AMP-PNP)	N.D.[a]	3		I-II
	aPKCι/Par6b	5.9 (4.4-8.0)	3		I-V
	aPKCι/Par6b (Mg/ADP)	7.4 (6.1-8.9)	4		I-V
	aPKCι/Par6b (Mg/AMP-PNP)	9.7 (8.2-13.3)	9		I-V
	aPKCι/Par6b(ΔCT)	14 (10.7-18.2)	3	V	I-IV
	aPKCι/Par6b(ΔCT) (Mg/ADP)	18.8 (14.3-24.9)	3	V	I-IV
	aPKCι(PB1)/Par6b	11.3 (9.7-13.3)	3		III-V
	aPKCι(PB1)/Par6b(ΔCT)	N.D.[a]	3	V	III, IV
	GST-Par6b(CBD)	5843 (4119-8261)	3		V
	aPKCι/Par6a	7.0 (4.5-11.0)	3		I-V
	aPKCι/Par6a (Mg/ADP)	25.2 (20.4-31.1)	3		I-V
	aPKCι/Par6a (Mg/AMP-PNP)	24.4 (18.5-32.1)	4		I-V
	aPKCι(PB1)/Par6a	N.D.[a]	3		III-V
pLgl2s	aPKCι	N.D.[a]	3		I-II
	aPKCι/Par6b	7.0 (6.0-8.2)	3		I-V
	aPKCι/Par6b(Mg/AMP-PNP)	39.6 (28.3-55.0)	2		I-V
	aPKCι/Par6b(ΔCT)	2904 (2326-3627)	3	V	I-IV
	aPKCι/Par6a	272.9 (215.3-345.3)	3		I-V
Lgl2s(I700D)	aPKCι(PB1)/Par6b	227.6 (190.1-272.1)	3	IV	III, V
Lgl2s(Δ680-710)	aPKCι/Par6b	6.8 (5.5-8.4)	3	IV	I-V
	aPKCι/Par6b (Mg/ADP)	105.1 (82.0-134.2)	3	IV	I-V
	aPKCι(PB1)/Par6b	211.5 (181.5-246.1)	5	IV	III, V
Lgl2s(Δ10-11)	aPKCι(PB1)/Par6b	198.8 (172.3-229.2)	3	IV	III, V
	aPKCι(PB1)/Par6b(ΔCT)	N.D.[a]	3	IV, V	III
	aPKCι	5772 [b] (1933-9611)	8	I	II
Lgl2s(3KA)	aPKCι(PB1)/Par6b	N.D.[a]	3	V	III, IV
	GST-Par6b(CBD)	N.D.[a]	3	V	-
Lgl2(626-680)	aPKCι	2540 (2064-3127)	3		I
	aPKCι/Par6b	2292 (1910-2743)	3		I

Values in parenthesis represent the dissociation constant's confidence intervals at 95% confidence level.

Binding parameters were fitted to results from experiments repeated *n* times.

For the binding experiments with Lgl2, the effect of the mutations/deletions tested on the different binding interfaces with aPKCι/Par6b (sites I-V) is denoted.

[a] Not detected. Low-affinity binding (>micromolar) could not be quantified due to non-specific binding at very high concentrations.

[b] Value is the mean of K_D fit results, determined individually for each repetition using one-site saturation with non-specific binding.

Table 2. Summary table of fluorescence polarization binding experiments.

	Lgl2/aPKCι/Par6b (nucleotide-free)		Lgl2/aPKCι/Par6b (ADP-bound)	Lgl2/aPKCι/Par6a (nucleotide-free)	Lgl2/aPKCι/Par6a (ADP-bound)
Data collection and processing					
Microscope	Titan Krios		Titan Krios	Titan Krios	Titan Krios
Electron Detector	Gatan K3		Gatan K3	Gatan K3	Gatan K3
Voltage (kV)	300 kV		300 kV	300 kV	300 kV
Magnification	X81,000		X81,000	X81,000	X81,000
Electron exposure (e–/Å^2)	65		65	65	65
Defocus range (μm)	-1.0 to -4.0		-1.3 to -3.5	-1.1 to -2.9	-1.2 to -3.5
Pixel size (Å)	1.111		1.111	1.111	1.111
Tilt angle (°)	25/40		25/40	40	25/40
Initial particle images at each angle (no.	1,373,256 / 1,304,615		621,404 / 1,304,114	535,165	373,437 / 346,141
	"Headless"	"Headed"			
Final particle images (no.)	1,391,872	251,742	787,439	95,801	357,297
Map resolution (Å)	3.08	3.48	3.33	4.05	3.31
FSC threshold	0.143	0.143	0.143	0.143	0.143
Symmetry imposed	C1	C1	C1	C1	C1
Model Building and Refinement					
Initial models used (PDB codes)	6N8Q, 6LI1, 1NF3	6N8Q, 6LI1, 1NF3, 1WMH	6N8Q, 6LI1, 1NF3		
Map sharpening B factor (Å^2)	-159.3	-136.7	-176.1	-137.8	-128.4
Model composition					
Non-hydrogen atoms	9,854	11,764	10,056		
Protein residues	1,293	1,564	1,301		
Ligands			1(Mg), 1(ADP)		
B factors (Å^2)					
Protein	64.77	84.14	66.87		
Ligand			57.91		
R.M.S. deviations					
Bond lengths (Å)	0.002	0.003	0.002		
Bond angles (°)	0.492	0.558	0.502		
Validation					
MolProbity score	1.47	1.61	1.48		
Clashscore	3.71	4.62	4.73		
Poor rotamers (%)	0.49	0.60	0.85		
Ramachandran plot					
Favored (%)	95.50	95.38	96.47		
Allowed (%)	4.50	4.62	3.53		
Disallowed (%)	0.00	0.00	0.00		

Table 3. Cryo-EM data collection, structure determination, and model refinement.

Protein construct	Plasmid	Expression	Gene	Range	Mutations	N' fusion	C' fusion
Lgl2s	pVL-1393	Insect (SF9)	Human Lgl2 (Q6P1M3)	13-978		S	EFTTSAS-[TEV]-[Protein-A]
Lgl2s-6H	pVL-1393	Insect (SF9)	Human Lgl2 (Q6P1M3)	13-978		S	EFTTSAS-[6H]-[TEV]-[Protein-A]
3G-Lgl2s	pVL-1393	Insect (SF9)	Human Lgl2 (Q6P1M3)	13-978	I700D	[TEV]GGS	EFTTSAS-[TEV]-[Protein-A]
3G-Lgl2s(I700D)	pVL-1393	Insect (SF9)	Human Lgl2 (Q6P1M3)	13-978	I700D	[TEV]GGS	EFTTSAS-[TEV]-[Protein-A]
3G-Lgl2s(3KA)	pVL-1393	Insect (SF9)	Human Lgl2 (Q6P1M3)	13-978	K820A/K832A/K834A	[TEV]GGS	EFTTSAS-[TEV]-[Protein-A]
3G-Lgl2s(Δ680-710)	pVL-1393	Insect (SF9)	Human Lgl2 (Q6P1M3)	13-978	Δ680-710	[TEV]GGS	EFTTSAS-[TEV]-[Protein-A]
3G-Lgl2s(Δ10-11)	pVL-1393	Insect (SF9)	Human Lgl2 (Q6P1M3)	13-978	Δ629-710	[TEV]GGS	EFTTSAS-[TEV]-[Protein-A]
aPKCι	pAcHLT-A	Insect (SF9)	Human aPKCi (P41743)	1-596		[6H]GRRRASVAAGI[TRB]PGLD[TEV]G	
aPKCι/Par6a	pVL-Dual*	Insect (SF9)	Human aPKCi (P41743)	1-596			
			Human Par6A (Q9NPB6-2)	1-345			EFTTSAS-[TEV]-[Protein-A]
aPKCι/Par6b	pVL-Dual*	Insect (SF9)	Human aPKCi (P41743)	1-596			
			Mouse Par6B (AAF71528)	1-371			EFTTSAS-[TEV]-[Protein-A]
aPKCι/Par6a(ΔCT)	pVL-Dual*	Insect (SF9)	Human aPKCi (P41743)	1-596			
			Human Par6A (Q9NPB6-2)	1-252			EFTTSAS-[TEV]-[Protein-A]
aPKCι/Par6b(ΔCT)	pVL-Dual*	Insect (SF9)	Human aPKCi (P41743)	1-596			
			Mouse Par6B (AAF71528)	1-253			EFTTSAS-[TEV]-[Protein-A]
aPKCι(PB1)/Par6a	pVL-Dual*	Insect (SF9)	Human aPKCi (P41743)	1-108		[6H]GSGS	
			Human Par6A (Q9NPB6-2)	1-345			EFTTSAS-[TEV]-[Protein-A]
aPKCι(PB1)/Par6b	pVL-Dual*	Insect (SF9)	Human aPKCi (P41743)	1-108		[6H]GSGS	
			Mouse Par6B (AAF71528)	1-371			EFTTSAS-[TEV]-[Protein-A]
	pVL-Dual*	Insect (SF9)	Human aPKCi (P41743)	1-108		[6H]GSGS	
			Mouse Par6B (AAF71528)	1-253			EFTTSAS-[TEV]-[Protein-A]
aPKCι-Ink-Par6a	pVL-1393	Insect (SF9)	Human aPKCi (P41743)	1-596			[3C]GGG[6H]GGGGS[3C]
			Human Par6A (Q9NPB6-2)	1-345			EFTTSAS-[TEV]-[Protein-A]
aPKCι-Ink-Par6b	pVL-1393	Insect (SF9)	Human aPKCi (P41743)	1-596			[3C]GGG[6H]GGGGS[3C]
			Mouse Par6B (AAF71528)	1-371			EFTTSAS-[TEV]-[Protein-A]
GST-Par6b-CT	pGEX-2T	E.coli	Mouse Par6B (AAF71528)	254-371		[GST]-SD[TRB]ICGGGG[TEV]GI	
GST-hPar6b-CT	pGEX-2T	E.coli	Human Par6b (Q9BYG5)	254-372		[GST]-SD[TRB]ICGGGG[TEV]GI	
GST-hPar6b-CT (I307N)	pGEX-2T	E.coli	Human Par6b (Q9BYG5)	254-372	I307N	[GST]-SD[TRB]ICGGGG[TEV]GI	
GST-hPar6b-CBD	pGEX-2T	E.coli	Human Par6b (Q9BYG5)	289-312		[GST]-SD[TRB]ICGGGG[TEV]GI	
Lgl2(626-680)	pCDF-Duet	E.coli	Human Lgl2 (Q6P1M3)	626-680		[6H]GS[MBP][TEV]	

[6H] = HHHHHH, [TEV] = ENLYFQ^G, [TRB] = LVPR^GS, [3C] = LEVLFQ^GP

* A PVL- based dual expression vector.

Table 4. DNA constructs.

Substrate	Sequence	Par6b	Km (μM)	Kcat (s^{-1})	K_D (μM)
Lgl2(626-680)	CTLHPSDQLALEGPLSRVKSLKKSLRQSFRR MRRSRVSSRKRHPAGPPGEAQEGS	-	1.62 ± 0.39	0.80 ± 0.05	2.5±0.3[a]
		+	1.14 ± 0.28	0.79 ± 0.05	
EPSS	ERMRPRKRQGSVRRRVHQVN	-	4.93 ± 0.55	0.75 ± 0.02	13.3±2.1[b]
		+	2.34 ± 0.16	0.97 ± 0.02	
Par1(602-621)	TRFPRGSSSRSTFHGEQLRE	-	60.24 ± 5.08	0.60 ± 0.02	
		+	19.96 ± 1.36	0.91 ± 0.02	

[a] Measured by FP.

[b] Reported by Soriano et al., 2016.

Table 5. Catalytic activity of aPKCι with different substrate peptides.